

# Development of a micro catalytic combustor using high-precision ceramic tape casting

Takashi Okamasa<sup>1</sup>, Gwang-Goo Lee<sup>1</sup>, Yuji Suzuki<sup>1</sup>,  
Nobuhide Kasagi<sup>1</sup> and Shin Matsuda<sup>2</sup>

<sup>1</sup> Department of Mechanical Engineering, The University of Tokyo, 7-3-1 Hongo, Bunkyo-ku, Tokyo 113-8656, Japan

<sup>2</sup> Kyocera Corp., Kokubu Plant 1-1 Yamashita-cho, Kokubu, Kagoshima 899-4396, Japan

E-mail: [okamasa@thtlab.t.u-tokyo.ac.jp](mailto:okamasa@thtlab.t.u-tokyo.ac.jp)

Received 20 February 2006, in final form 31 May 2006

Published 9 August 2006

Online at [stacks.iop.org/JMM/16/S198](http://stacks.iop.org/JMM/16/S198)

## Abstract

A micro-scale catalytic combustor fueled by butane was investigated. High-precision ceramic tape-casting technology was adopted for developing a three-dimensional structure of the combustor with embedded heat exchange channels. Nano-porous alumina fabricated through anodic oxidation of aluminum layers was employed for the support of Pd catalyst. Combustion experiments were carried out in a solder bath to keep the catalyst temperature constant. Complete fuel conversion for a n-butane flow rate of 5.0 sccm has been achieved at 390 °C corresponding to 100 MW m<sup>-3</sup> heat generation. Reaction constants for catalytic combustion on the Pd/nano-porous alumina were determined with the aid of a 1D plug flow model. Those parameters were successfully combined with a CFD analysis to investigate the detailed transport phenomena and to predict the performance of the combustor at higher temperature. It was also shown in a preliminary experiment in air that the reaction can be self-sustained at 425 °C with the n-butane flow rate of 15 sccm.

## 1. Introduction

Due to recent advances in mobile electronic devices and autonomous robots, the worldwide demand for secondary batteries is growing rapidly. Although the Li-ion battery has the highest energy density among secondary batteries for consumer use at present, it is expected that its energy density is far below the need of the high-performance electronic devices in the near future. On the other hand, the energy density of hydrocarbon fuels such as methanol, propane and butane is tens of times larger than that of the Li-ion battery. Therefore, miniaturized energy conversion from chemical energy of hydrocarbon fuels to electricity attracts much attention [1].

In the present study, we investigate a small-scale combustor, which is essential for various mobile power generation systems such as gas turbine engine [2], thermoelectric generator [3], thermophotovoltaic (TPV) generator [4] and reformer-based fuel cell [5]. The advantage of combustion-based systems over fuel cells is their higher

electrical generation density. In order to avoid quenching phenomena due to the increase of the surface-to-volume ratio in small-scale combustors, excess-enthalpy combustors [6–8] and a combustor with proper wall material and temperature conditions [9] are proposed. However, catalytic combustion is preferred to homogeneous combustion due to the potential of stable heat generation with better controllability in the range of tens of watts [10]. Arana *et al* [11] developed a micro suspended-tube chemical reactor with Pt catalyst for high-temperature fuel processing. They obtained 0.8 W heat generation using butane fuel with extremely small heat loss to the ambient. Vican *et al* [7] developed a Swiss-roll type micro combustor to reduce heat loss to ambient. They employed platinum/alumina as the catalyst, and made combustion experiments using hydrogen over a wide range of equivalence ratios. Ahn *et al* [12] also developed a Swiss-roll combustor to investigate the reaction characteristics with and without platinum catalyst. They reported that catalytic combustion could extend the flammability limit to extremely

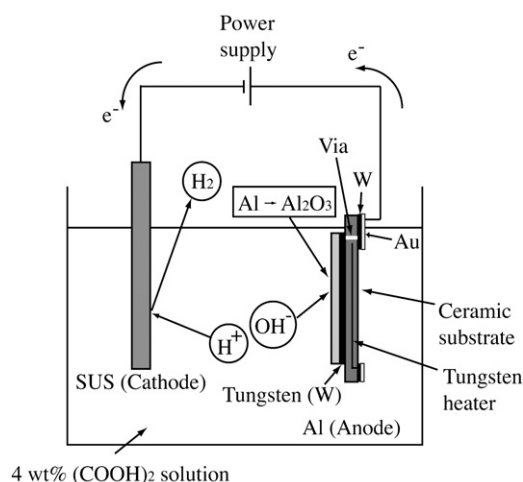


**Figure 1.** Schematic of anodic oxidation bath.

low temperatures around 80 °C. Wang *et al* [13] developed a micro ceramic combustor using a tape-casting method, and measured fuel conversion efficiency of n-butane on palladium/alumina catalyst under low-temperature conditions (<700 K). In our previous study on micro-scale combustion using a 0.6 mm ID tube, Suzuki *et al* [14] demonstrated that anodized nano-porous alumina is promising as the support of a platinum catalyst.

The objective of the present study is to develop a high-performance micro-scale catalytic combustor, which can be applied to micro TPV systems. Since the target temperature is above 800 °C, a palladium (Pd) catalyst supported by nano-porous alumina is employed. A high-precision ceramic tape-casting technology [15] is employed for the fabrication of the combustor equipped with heat exchange channels. A series of experiments with normal butane (n-butane) was carried out, and the performance of the combustor is discussed through comparisons between the experimental data and the CFD results.

## 2. Fabrication

### 2.1. Catalyst layer

In the present study, nano-porous alumina made through anodic oxidation of aluminum is employed as the catalyst support [16]. Advantages of the anodized alumina support are twofold; firstly, it is easy to optimize the film thickness and its characteristics such as porosity and pore diameter. Secondly, anodized alumina has good adhesion to the substrate, so that the catalyst layer is robust for thermal shock expected to occur during the operation of micro combustors. Suzuki *et al* [15] employed time-consuming thermal evaporation for the deposition of the aluminum layer. In the present study, we employ thermal spray coating instead in order to fabricate thick aluminum layers more efficiently. We employ a Pd catalyst, because a Pd catalyst can be used up to 900 °C and has larger active surface area than Pt at temperatures above 600 °C.

The fabrication process of Pd/nano-porous alumina starts with the deposition of about 100  $\mu\text{m}$  thick aluminum onto a tungsten film on a ceramic substrate using thermal spray coating. The porosity of the aluminum layer is about 1%.

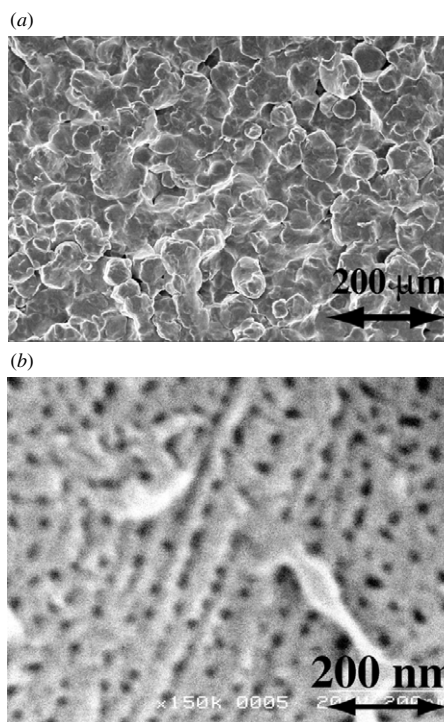


**Figure 2.** SEM images of catalyst support. (a) Aluminum layer as deposited with thermal spray coating. (b) Nano-porous alumina surface after anodic oxidation.

The substrate is then annealed in nitrogen gas at 500 °C for 5 h to improve adhesion between the tungsten and aluminum films. Then, the substrate is submerged in an anodic oxidation bath (figure 1), in which a 4 wt% oxalic acid solution is employed as the electrolyte. The temperature of the solution is kept at 10 °C. A constant current source and a stainless steel rod are respectively employed for the power supply and the cathode. Electric current density and the duration of anodic oxidation are respectively chosen as 50  $\text{A m}^{-2}$  and 7 h, which are enough to anodize the entire aluminum layer. Note that electronic contact to the aluminum layer is accomplished with the base tungsten layer, which has a contact through a via to the backside gold-plated tungsten pad. After the anodic oxidation, a bake at 350 °C is made for 1 h in nitrogen gas. Finally, the nano-porous alumina is dipped into 4.5 wt% diamine-dinitropalladium solution ( $\text{Pd}(\text{NH}_3)_2(\text{NO}_2)_2$ ) at 50 °C for 1.5 h, dried naturally for 2 h and calcinated at 350 °C for 1 h in nitrogen gas. Kameyama *et al* [17] report that the surface area of the alumina prepared with the above-mentioned procedure can be increased up to over 150  $\text{m}^2 \text{g}^{-1}$  after calcination.

Figure 2(a) shows a SEM image of the aluminum layer deposited with the thermal spray coating. Since the aluminum particles employed have a diameter of around 20  $\mu\text{m}$ , the surface roughness of the aluminum layers is a few tens of micrometers. After the anodic oxidation, the surface has a nano-porous structure, where the pore diameter and the mean spacing between pores are respectively 20 nm and 50 nm as shown in figure 2(b).

### 2.2. Ceramic micro combustor

In order to fabricate a cost-effective and robust micro-scale combustor, we employ high-precision tape-casting technology

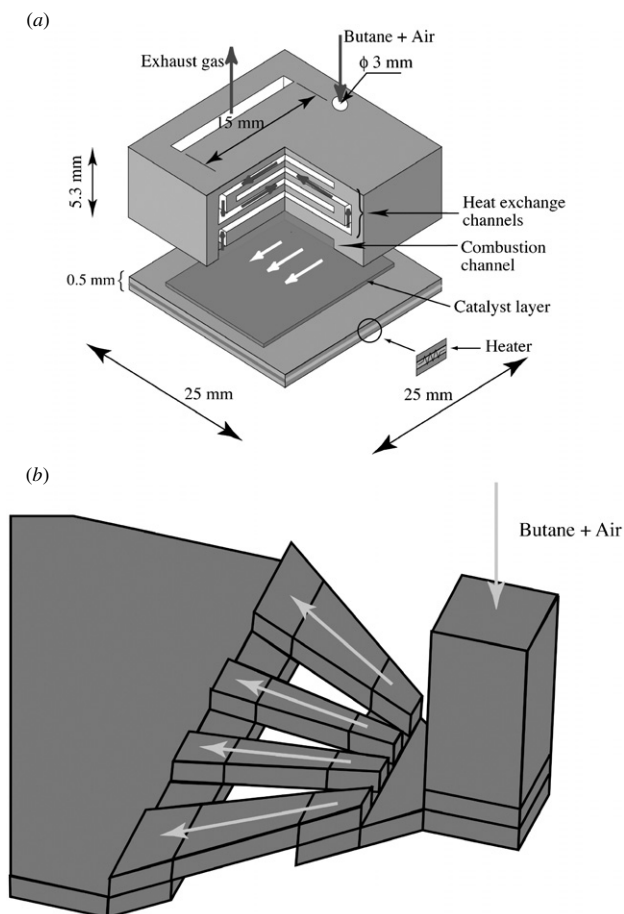


**Figure 3.** (a) Schematic of micro-scale ceramic combustor with embedded heat exchange channels. (b) Schematic of the 3D manifold for uniform velocity distribution [15].

[15] developed for semiconductor ceramic packages. Its advantages are high thermal resistance, high-precision fabrication with an alignment error within  $30\ \mu\text{m}$ , applicability to quasi three-dimensional structures by stacking multiple layers, and simple integration of electrodes and heaters into the ceramic structure. In particular, the combustor fabricated by this technology has a potential for high-temperature operation up to  $800\ ^\circ\text{C}$ , which is determined by the brazing temperature of the ceramic plates.

Figure 3(a) shows a schematic design of the micro-scale ceramic combustor. For heat recovery, this prototype combustor has cross-flow heat exchange channels having cross sections of  $15 \times 0.5\ \text{mm}^2$ . Through these channels, heat exchange takes place between the fresh mixture and high-temperature exhaust gas. Surface reaction of n-butane occurs in the undermost combustion channel, of dimensions  $15 \times 19 \times 0.3\ \text{mm}^3$ . As shown in figure 3(b), the present combustor has a 3D manifold to achieve a uniform flow velocity profile in the cross-stream direction with minimal pressure drop. Due to multiple flow impingements to the manifold walls, the velocity at the center of the channel is uniform within 3% [15].

Figure 4(a) shows a birds-eye view of the micro ceramic combustor, which is fabricated by stacking 12 ceramic plates; the upper nine plates for the cross-flow heat exchange channels and the lower three plates for the combustion channel as

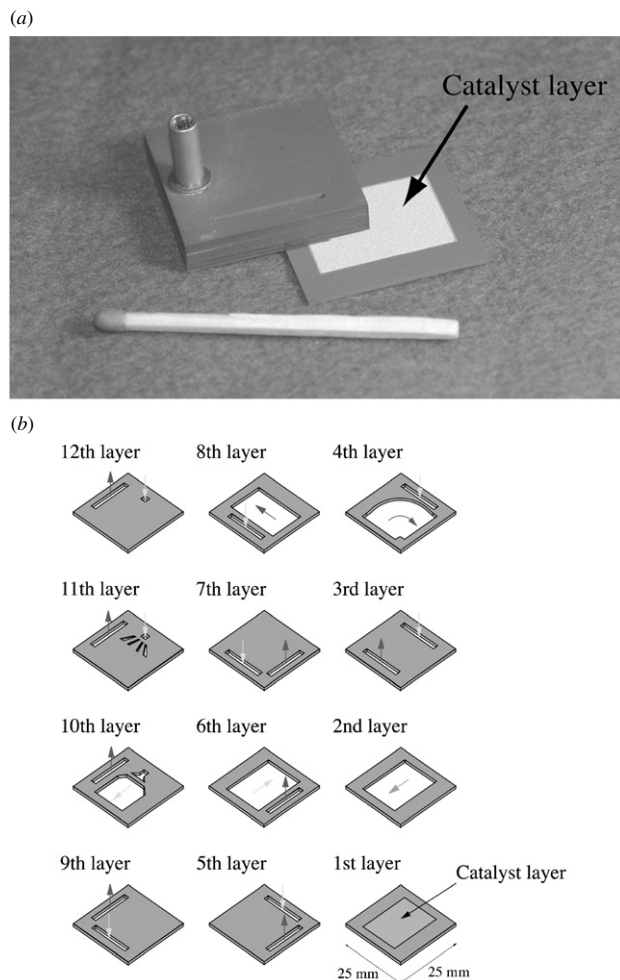


**Figure 4.** (a) Photograph of micro ceramic combustor prototype. (b) Schematic of an exploded view.

shown in figure 4(b). The thickness of the plates is chosen as 0.3–0.5 mm. The bottom plate (first layer) consists of two separate plates and an embedded tungsten heater for ignition in between. Two gold-plated tungsten pads are located on the backside of the bottom plate for the electrical connection to the heater. As shown in figure 1, the bottom plate also has another pad on the backside for anodic oxidation, which has via holes to the front-side electrode.

### 3. Combustion experiment

#### 3.1. Experimental setup

Figure 5 shows a schematic of the present experimental setup. Flow rates of n-butane and air are regulated by mass flow controllers (MASFLO, Oval Corp.). The full scales of these mass flow controllers are respectively 30 sccm and 1000 sccm for n-butane and air. Bias errors of the flow rate are within 1% of their full scale. Fuel and air are well mixed in the mixing section before entering the combustor. The combustor is submerged into a solder bath in order to keep the catalyst temperature constant at  $200\text{--}400\ ^\circ\text{C}$ . Since solder has a large heat capacity and thermal conductivity, the temperature

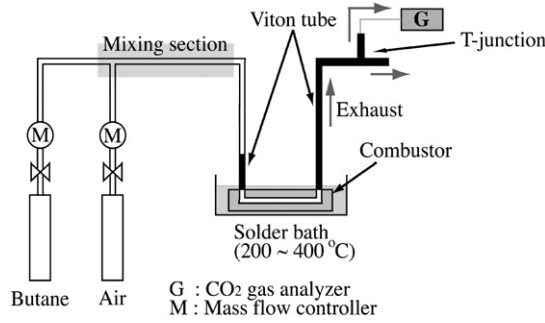


Figure 5. Experimental setup.

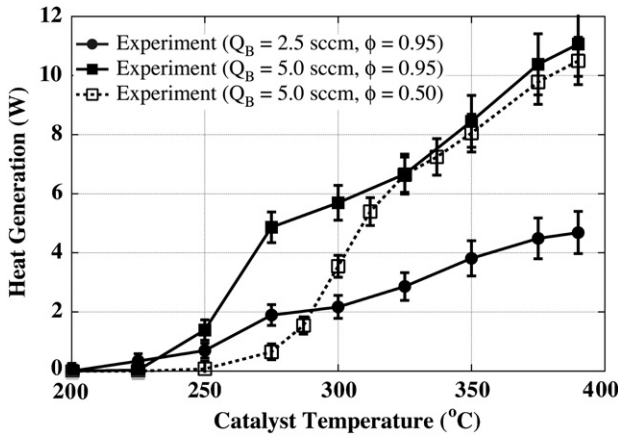


Figure 6. Heat generation versus catalyst temperature.

difference between the catalyst and the solder is estimated to be within 11 K for the butane flow rate of 5.0 sccm.

The fuel conversion efficiency is evaluated with the carbon dioxide concentration in the exhaust gas. Since the aspiration rate of the gas analyzer (Model 4300, Nippon Thermo) is larger than the flow rate of the exhaust gas, ambient air is also introduced into the gas analyzer through a T-junction shown in figure 5. The CO<sub>2</sub> concentration of the exhaust gas is compensated using the flow rate of the exhaust gas and the aspiration rate of the gas analyzer. The bias error of the gas analyzer is within 0.5% of its full scale. Under the present experimental condition, the flow rate of n-butane  $Q_B$  is changed in the range of 2.5–5.0 sccm corresponding to the heat generation of 5–10 W at complete fuel conversion. The equivalence ratio  $\phi$  is maintained constant at 0.95 when  $Q_B$  is 2.5 sccm, and changed in the range of 0.5–0.95 when  $Q_B$  is 5.0 sccm. The Reynolds number is 10–60 under the present experimental conditions, so that the flow in the combustor remains laminar.

### 3.2. Experimental results

Prior to combustion experiments, the palladium catalyst is activated by reduction using 1 vol% hydrogen gas at 300 °C for 10 h, and the combustor is operated for a sufficiently long period to reach the steady activation state. Figure 6 shows heat generation versus the catalyst temperature. Each data point represents an ensemble average over 27 samples for 13 min. The uncertainty intervals ( $U_{\text{rss}} = 95\%$ ) are calculated with the

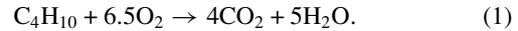
measurement uncertainty of the mass flow rate, the aspiration rate of the gas analyzer, and the CO<sub>2</sub> concentration. It is found that onset of ignition is in between 225 °C and 250 °C, and the heat generation increases with the catalyst temperature. When  $\phi = 0.95$ , the fuel conversion efficiency for  $Q_B = 2.5$  and 5.0 sccm is respectively  $94 \pm 14\%$  and  $110 \pm 11\%$  at 390 °C. Therefore, almost complete fuel conversion has been achieved under these conditions. Note that efficiency larger than 100% is due to the measurement uncertainty, but 100% efficiency is still within the uncertainty interval. For  $Q_B = 5.0$  sccm, the heat generation is 10 W, which corresponds to heat generation density as large as  $100 \text{ MW m}^{-3}$ .

When  $Q_B = 5.0$  sccm and  $\phi = 0.50$ , the fuel conversion efficiency is  $105 \pm 10\%$  at 390 °C. Thus the reduction of the equivalence ratio from 0.95 to 0.5, which corresponds to the decrease in the residence time, gives small changes in the fuel conversion efficiency. Therefore, diffusion in the combustion channel is not the limiting factor, but the surface reaction speed itself plays a dominant role in determining the overall reaction rate at low catalyst temperature.

## 4. Modeling and CFD analysis

### 4.1. Surface reaction model

While simple but reasonable surface reaction models are proposed for hydrogen and methane [18], the detailed surface reaction mechanism of n-butane remains unknown because of its complex elementary reaction steps. In the present study, we assume the one-step irreversible reaction of n-butane, i.e.,



In addition, since the oxidation rate of hydrocarbons on a catalyst is typically modeled as the first order in fuel a concentration and independent of oxygen concentration [13, 19], the surface reaction rate of n-butane,  $R_B$ , can be expressed as

$$R_B = C_{B,s}(x) \cdot A \cdot \exp\left(-\frac{E}{RT_c}\right), \quad (2)$$

where  $C_{B,s}(x)$ ,  $A$ ,  $E$ ,  $R$  and  $T_c$  are respectively the molecular concentration of butane at the catalyst surface, pre-exponential factor, activation energy, universal gas constant and catalyst temperature. The reaction constants, i.e.,  $A$  and  $E$ , are dependent on the effective surface area and the activity of the catalyst, and should be determined from the experimental data. In the present study, the 1D plug flow model is assumed, which is based on the assumption of no mixing in the streamwise direction but perfect mixing in the transverse direction. With this model, mole balance equations of n-butane can be written as

$$A_c \frac{du C_{B,b}(x)}{dx} + W k_{m,B}(C_{B,b}(x) - C_{B,s}(x)) = 0, \quad (3)$$

$$k_{m,B}(C_{B,b}(x) - C_{B,s}(x)) = R_B, \quad (4)$$

where  $A_c$ ,  $u$ ,  $C_{B,b}(x)$ ,  $W$  and  $k_{m,B}$  are respectively the cross-sectional area of the combustion channel, bulk mean velocity, bulk mean concentration of n-butane at the streamwise position of  $x$ , wetted area per unit length and mass transfer rate of

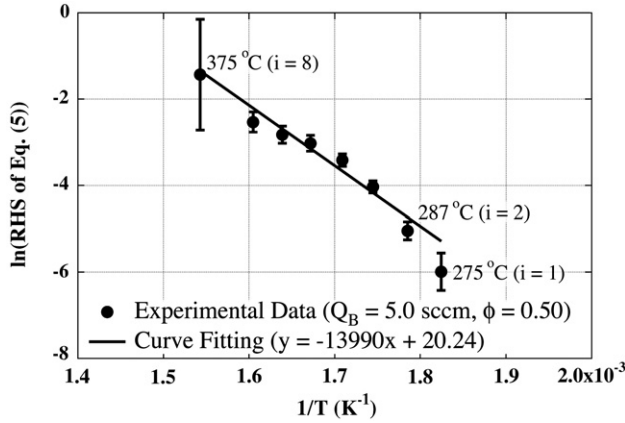


**Figure 7.** Temperature dependence of the specific reaction rate for  $Q_B = 5.0$  sccm and  $\phi = 0.50$ .

n-butane. From equations (3) and (4), we obtain

$$A \exp\left(-\frac{E}{RT_c}\right) = -\frac{uA_c}{WL} \ln\left(\frac{C_{B,b}(L)}{C_{B,b}(0)}\right) \left[1 + \frac{uA_c}{Wk_{m,B}L} \ln\left(\frac{C_{B,b}(L)}{C_{B,b}(0)}\right)\right], \quad (5)$$

where  $L$  is the streamwise length of the catalyst layer [14]. In the derivation of equation (5), the bulk mean velocity is assumed constant in the streamwise direction, because its change due to chemical reaction is less than 4.7%. Assuming a fully developed mass boundary layer with the Sherwood number equal to 4 [20], the mass transfer rate,  $k_{m,B}$ , can be given by

$$k_{m,B} = \text{Sh} \cdot \frac{D_B}{d} \sim 4 \cdot \frac{D_B}{d}, \quad (6)$$

where  $D_B$  and  $d$  are the mass diffusivity of n-butane in air and the hydraulic diameter of the combustion channel. Since the mole concentration of n-butane is small enough under present experimental conditions,  $D_B$  is independent of the n-butane concentration. Then  $D_B$  can be given by

$$D_B = 8.67 \times 10^{-6} \left(\frac{T}{273}\right)^{1.833}. \quad (7)$$

We can determine all the variables on the RHS of equation (5) from the combustor dimensions and the experimental data. Figure 7 shows the RHS of equation (5) versus  $1/T$ , where error bars represent the uncertainty intervals. We employ the experimental data for  $Q_B = 5.0$  sccm and  $\phi = 0.50$  in order to determine the reaction constants with a curve fitting, because the uncertainty interval of the fuel conversion efficiency is the smallest among the three experimental conditions. We apply a weighted least-squares method to the experimental data between 275 and 375 °C with a weighted factor  $W_i$  ( $i = 1, \dots, 8$ ) given by

$$W_i = \frac{\left(\frac{1}{U_i}\right)^2}{\sum_{i=1}^8 \left(\frac{1}{U_i}\right)^2}, \quad (8)$$

where  $U_i$  represents the uncertainty interval of each data point. From the y-intercept and the slope, we obtain the reaction constants as follows:  $A = 6.181 \times 10^8$  ( $\text{m s}^{-1}$ ) and  $E = 1.163 \times 10^8$  ( $\text{J kmol}^{-1}$ ). The activation energy estimated in the present study is in reasonable agreement with the previous data by Wang *et al* [13] of  $0.9 \pm 0.05 \times 10^8$  ( $\text{J kmol}^{-1}$ ).

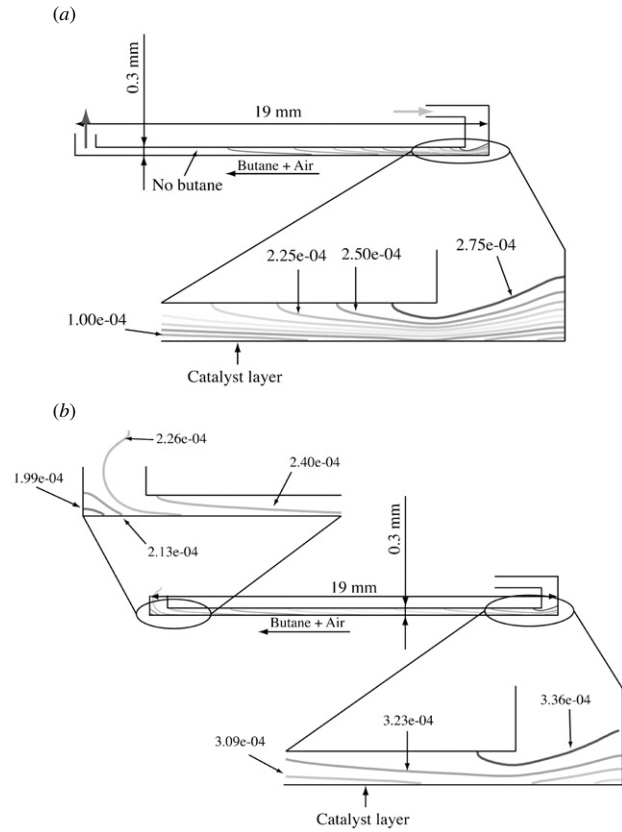


**Figure 8.** Iso-contours of n-butane molar concentration in the longitudinal symmetry plane of the combustion channel for  $Q_B = 5.0$  sccm and  $\phi = 0.50$ . (a) Catalyst temperature of 390 °C. (b) Catalyst temperature of 300 °C.

#### 4.2. CFD analysis of the ceramic combustor

With the reaction constants of the surface reaction model, we made a series of CFD analysis of the flow, thermal and concentration fields with commercial software (Fluent 6, Fluent Inc.). In addition to the Navier–Stokes equations, the energy and species transport equations in the flow domain, and the heat conduction equation in the ceramic wall are solved. Temperature dependence of density, specific heat and mass diffusivity for the mixture are considered. As mentioned earlier, the flow inside the combustor remains laminar. The temperature of the catalyst wall is set constant, and all the external surfaces of the combustor excluding the inlet and the outlet are assumed to be thermally insulated. At the inlet, the temperature of the butane–air mixture is set to 300 K and a uniform velocity profile is assumed. The outflow boundary condition is assumed at the outlet. The thermal conductivity of the ceramic walls is set to  $14 \text{ W mK}^{-1}$ .

Figure 8 shows contours of n-butane molar concentration in the longitudinal symmetry plane of the combustion channel for  $Q_B = 5.0$  sccm at  $\phi = 0.50$ . For the catalyst temperature of 390 °C, the gradient of the molar concentration is large in the wall-normal direction as shown in figure 8(a). Since almost perfect conversion is achieved in this case, the molar concentration is very small near the channel exit. On the other hand, at a lower temperature of 300 °C, contours are sparsely distributed due to lower reaction rate, and about 70%

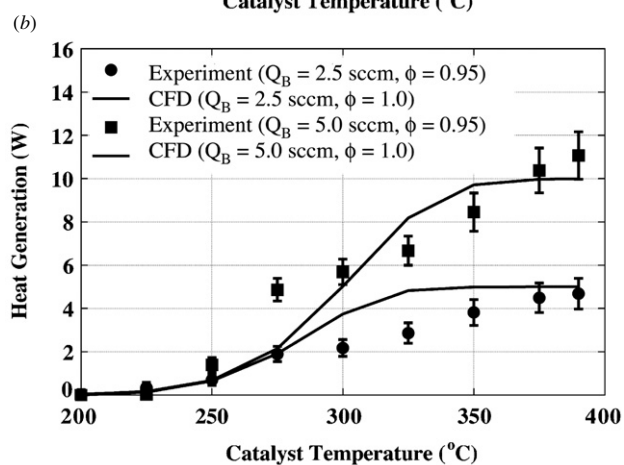
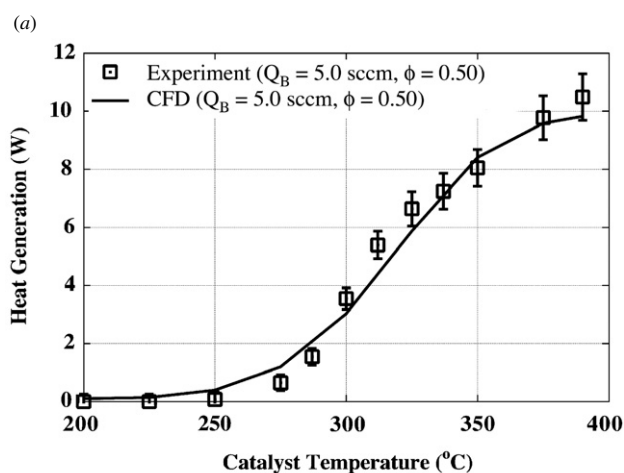


**Figure 9.** Comparison between the experimental data and CFD results. (a)  $Q_B = 5.0$  sccm and  $\phi = 0.50$ , (b)  $Q_B = 2.5$  and  $5.0$  sccm and  $\phi = 0.95$ .

of the fuel leaves the combustion channel (figure 8(b)) without reaction.

CFD results of the heat generation are compared with the experimental data. Figure 9(a) shows heat generation for  $Q_B = 5.0$  sccm at  $\phi = 0.50$ . Since the experimental data at this particular fuel flow rate are used for the curve fitting, the CFD results are in good agreement with the experimental data. Figure 9(b) shows heat generation for  $Q_B = 2.5$  sccm and  $Q_B = 5.0$  sccm at  $\phi = 0.95$ . The CFD results are in accordance with the experimental data. However, the present CFD result somewhat overestimates the heat generation between  $325^\circ\text{C}$  and  $350^\circ\text{C}$  for both  $Q_B = 2.5$  and  $5.0$  sccm.

The performance of the present combustor at a higher catalyst temperature is estimated with the CFD analysis. Figure 10(a) shows the n-butane flow rate for 98.5% fuel conversion efficiency at  $\phi = 1.0$  versus the catalyst temperature  $T_c$ . At  $800^\circ\text{C}$ , n-butane flow rate of 24 sccm can be converted with 98.5% fuel conversion efficiency, which corresponds to as large as 47 W heat generation. Figure 10(b) shows the ratio of the diffusion rate to the specific reaction rate. The ratio is higher than 15 at  $T_c = 300^\circ\text{C}$ , but rapidly decreases with increasing  $T_c$ . It is found that the ratio becomes lower than unity for  $T_c > 380^\circ\text{C}$ . Therefore, the overall reaction rate is limited by diffusion for catalyst temperature higher than

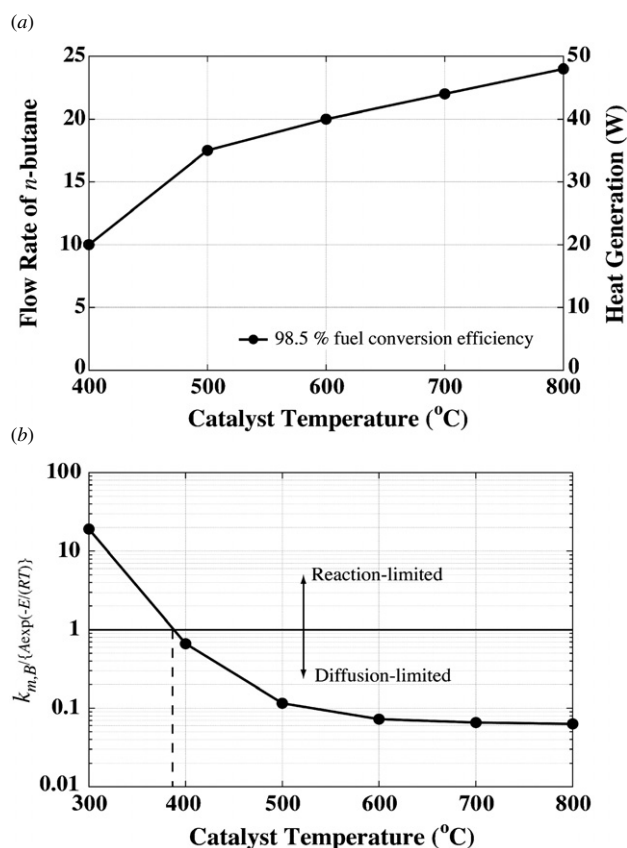


**Figure 10.** CFD prediction of the catalytic combustion for higher catalyst temperatures. (a) n-butane flow rate for 98.5% fuel conversion efficiency. (b) Ratio of the diffusion rate to the specific reaction rate.

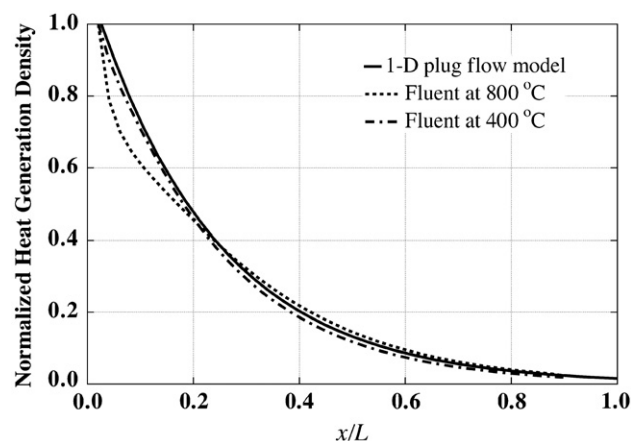


**Figure 11.** Distribution of normalized heat generation density in the streamwise direction for 98.5% fuel conversion efficiency.

$380^\circ\text{C}$ . This is why the fuel flow rate for 98.5% conversion is somewhat saturated for high catalyst temperature.

Figure 11 shows profiles of heat generation density in the streamwise direction for 98.5% fuel conversion efficiency. The vertical axis is non-dimensionalized with its value at the leading edge. When the 1D plug flow model is employed, distributions for the same fuel conversion efficiency are independent of the catalyst temperature  $T_c$  and collapse on

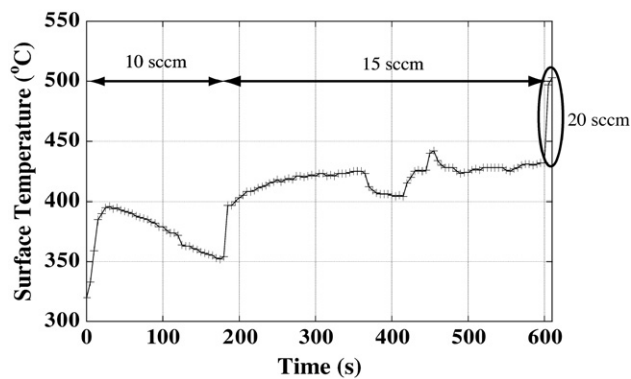


**Figure 12.** Time trace of the combustor surface temperature during a combustion experiment in the atmosphere.

a single curve; the heat generation density decays with an exponential curve in the streamwise direction. CFD results for  $T_c = 400$  and  $800$  °C show a small discrepancy near the inlet, but are in good agreement with profiles of the 1D plug flow model downstream. This large distribution of the heat generation density will result in nonuniform distribution of the catalyst temperature, which should be minimized in real applications such as TPV.

## 5. Preliminary experiment in the atmosphere

A preliminary experiment on combustion in the atmosphere is made to examine the sustainability of the present combustor. The temperature of the bottom surface of the combustor is measured by a radiation thermometer (TMZ51, Japan Sensor Corp.) with a measurement spot diameter of 3 mm. Figure 12 shows the time trace of the surface temperature. In this experiment, the equivalence ratio is kept at 0.95, and the n-butane flow rate is changed with time. The combustor is preheated up to  $300$  °C before fuel is supplied to the combustor. For  $Q_B = 10$  sccm, the surface temperature gradually decreases after unstable operation during the first tens of seconds, because heat loss by natural convection and thermal radiation is larger than the heat generation inside the combustor. On the other hand, for  $Q_B = 15$  sccm, self-sustained combustion is achieved with relatively small temperature change because of larger heat generation. Although there are temperature fluctuations with small amplitude, the temperature is restored to its original level. When  $Q_B = 20$  sccm, we can operate the combustor at higher temperature than  $500$  °C. With a 1D analysis, the catalyst temperature under this condition is estimated to be about  $505$  °C. It is noted that although the ceramic plate itself should withstand much higher temperature, this particular experiment was limited to  $500$  °C because of the low thermal durability of the tubing material and the brazing material.

## 6. Conclusion

A micro-scale catalytic combustor has been developed using a high-precision ceramic tape-casting technology. It is found that Pd/nano-porous alumina catalyst fabricated through anodic oxidation of spray-coated aluminum works well for

catalytic combustion of n-butane. The combustor performance is evaluated by a series of experiments in a solder bath. The Pd catalyst has shown high activity even at a low temperature around  $400$  °C. With a detailed analysis of combustion characteristics by CFD, the reaction constants are determined from the experimental data with the aid of a 1D plug flow model. It is suggested through the CFD analysis that for  $\phi = 1.0$ , up to 24 sccm n-butane is completely converted at  $800$  °C in the present combustor. A preliminary combustion experiment in air shows that stable operation is possible at  $425$  °C with the butane flow rate of 15 sccm.

## Acknowledgment

This work was supported by the New Energy and Industrial Technology Development Organization (NEDO) of Japan.

## References

- [1] Jacobson S A and Epstein A H 2003 An informal survey of power MEMS *Int. Symp. Micro-Mech. Eng. (Tsuchiura)* pp 513–20
- [2] Spadaccini C M, Zhang X, Cadou C P, Miki N and Waitz I A 2003 Preliminary development of a hydrocarbon-fueled catalytic micro-combustor *Sensors Actuators A* **103** 219–24
- [3] Itoigawa K, Ueno H, Shiozaki M, Toriyama T and Sugiyama S 2005 Fabrication of flexible thermopile generator *J. Micromech. Microeng.* **15** S233–8
- [4] Yang W, Chou S, Shu C, Xue H and Li Z 2005 Research on micro-thermophotovoltaic power generators with different emitting materials *J. Micromech. Microeng.* **15** S239–42
- [5] Tanaka S, Chang K, Min K, Satoh D, Yoshida K and Esashi M 2004 MEMS-based components of a miniature fuel cell/fuel reformer system *Chem. Eng. J.* **101** 143–9
- [6] Lloyd S A and Weinberg F J 1974 A burner for mixtures of very low heat content *Nature* **251** 47–9
- [7] Vican J, Gajdeczko B F, Dryer F L, Milius D L, Aksay I A and Yetter R A 2002 Development of a microreactor as a thermal source for microelectromechanical systems power generation *Proc. Combust. Inst.* **29** 909–16
- [8] Kim N I, Maruta K, Aizumi S, Yokomori T and Hasegawa S 2005 Development of small-scale Swiss-roll combustor and its scale effect *Proc. Power MEMS 2005* pp 202–5
- [9] Miesse C M, Masel R I, Jensen C D, Shannon M A and Short M 2004 Submillimeter-scale combustion *AIChE J.* **50** 3206–14
- [10] Fernandez-Pello A C 2002 Micropower generation using combustion: issues and approaches *Proc. Combust. Inst.* **29** 883–99
- [11] Arana L R, Schaevitz S A, Franz A J, Schmidt M A and Jensen K F 2003 A microfabricated suspended-tube chemical reactor for thermally efficient fuel processing *J. Microelectromech. Syst.* **12** 600–12
- [12] Ahn J, Eastwood C, Sitzki L and Ronney P D 2005 Gas-phase and catalytic combustion in heat-recirculating burners *Proc. Combust. Inst.* **30** 2463–72
- [13] Wang X, Zhu J, Bau H and Gorte R J 2001 Fabrication of micro-reactors using tape-casting methods *Catal. Lett.* **77** 173–7
- [14] Suzuki Y, Saito J and Kasagi N 2004 Development of micro catalytic combustor with Pt/ $\text{Al}_2\text{O}_3$  thin films *JSME Int. J. B* **47** 522–7
- [15] Suzuki Y, Horii Y, Kasagi N and Matsuda S 2004 Micro catalytic combustor with tailored porous alumina *Proc. 17th IEEE Int. Conf. MEMS (Maastricht)* pp 312–5

- [16] Sungkono I E, Kameyama H and Koya T 1997 Development of catalytic combustion technology of VOC materials by anodic oxidation catalyst *Appl. Surf. Sci.* **121/122** 425–8
- [17] Kameyama H, Murata K, Terai S and Toyoshima Y 1995 Development of plate type catalyst with anodic oxidation film of aluminum *J. Surf. Finish. Soc. Japan* **46** 425–8 (in Japanese)
- [18] Hickman D A and Schmidt L D 1993 Steps in CH<sub>4</sub> oxidation on Pt and Rh surfaces: high-temperature reactor simulations *AIChE J.* **39** 1164–77
- [19] Prasad R, Kennedy L A and Ruckenstein E 1984 Catalytic combustion *Catal. Rev. Sci. Eng.* **26** 1–58
- [20] Lee G G, Suzuki Y and Kasagi N 2006 Modeling of platinum catalyzed oxidation of butane in micro-scale combustors *Chem. Eng. Sci.* submitted